Journal of Geothermal Research and Volcanology (2026) 36-44

Contents lists available at FoundAE

Journal of Geothermal Research and Volcanology

Journal homepage: https://ejournal.foundae.com/index.php/jograv/index

# Gravity-based structural characterization of a radiogenic geothermal system in a non-volcanic setting: A case study from Pelawan, West Bangka, Indonesia

Meita Tasya Setiawan[a,*], Mikael Syväjärvi[b]

[a] Physical Sciences, Wahana Krida Konsulindo, Tangerang, Banten 15139, Indonesia
[b] Alminica AB, Ulrika, Östergötlands Län, Ulrika 59053, Sweden

ARTICLE INFO

*Keywords:*
Non-volcanic geothermal system
Subsurface structural interpretation
Structural control
Gravity modeling
Granite-hosted

ABSTRACT

Radiogenic geothermal systems represent a type of non-volcanic geothermal resource generated by the decay of radioactive elements within crystalline basement rocks, particularly granites. Despite Indonesia's well-known volcanic geothermal potential, radiogenic geothermal systems remain poorly investigated. This study presents a preliminary assessment of subsurface structures associated with the radiogenic geothermal signature in the Pelawan area, West Bangka Regency, using gravity data analysis. Secondary gravity and topographic datasets derived from the TOPEX satellite were processed to obtain Complete Bouguer Anomaly (CBA) values. Two-dimensional (2D) and three-dimensional (3D) gravity modeling were subsequently conducted to characterize subsurface density contrasts and identify structural features controlling geothermal manifestations. The gravity method is particularly suitable for distinguishing subsurface lithological variations based on density contrasts between anomalous bodies and surrounding formations. The modeling results reveal the presence of multiple fault structures surrounding the Pelawan geothermal manifestation, suggesting structural control of the geothermal system. The subsurface stratigraphy is interpreted to consist of Pleistocene alluvium (1.8–1.9 g/cm³), Triassic Tanjung Genting Formation (2.1 g/cm³), Triassic–Jurassic Klabat Granite (2.55 g/cm³), and the Pemali Formation as basement rock (2.6 g/cm³). The deeper sections of the model are dominated by granitic formations, which are interpreted as the primary radiogenic heat source. The identified fault structures are likely associated with granite intrusions and may act as pathways for geothermal fluid circulation. These findings provide new insights into the structural and lithological controls of radiogenic geothermal systems in non-volcanic settings in Indonesia and highlight the potential of the Pelawan area for further geothermal exploration.

## 1. Introduction

Geothermal energy is widely recognized as one of the most reliable and sustainable renewable energy resources due to its low greenhouse gas emissions and continuous availability independent of climatic conditions. In Indonesia, geothermal exploration has historically focused on volcanic and magmatic systems associated with the Pacific Ring of Fire [1, 2]. These high-enthalpy systems are typically linked to active tectonics and young volcanic complexes, which provide abundant heat sources derived from shallow magmatic intrusions. However, beyond volcanic geothermal systems, another class of geothermal resource—radiogenic geothermal—has received comparatively limited attention, particularly in Indonesia.

Radiogenic geothermal systems are classified as non-volcanic geothermal systems in which heat is primarily generated by the radioactive decay of naturally occurring isotopes such as uranium (U), thorium (Th), and potassium (K) within crystalline basement rocks. Granite and other felsic intrusive rocks are commonly enriched in these heat-producing elements, making them potential long-term sources of subsurface thermal energy [3–5]. Unlike magmatic geothermal systems, radiogenic systems are not necessarily associated with recent volcanic activity [6, 7]. Instead, they rely on the accumulation of radiogenic heat over geological time and are often controlled by lithological composition, structural discontinuities, and regional tectonic evolution [8–10].

* Corresponding author.
*E-mail address:* meitatasyasetiawan@gmail.com (M. T. Setiawan).

https://doi.org/10.58524/jograv.v1i1.108
Received 10 January 2026; Received in revised form 20 February 2026; Accepted 28 February 2026
Available online 10 March 2026
XXXX-XXXX/Published by FoundAE (Foundation of Advanced Education).

Globally, radiogenic geothermal systems have been investigated in regions characterized by granitic basement complexes, including Australia, Europe, and parts of Asia. These systems are commonly associated with enhanced geothermal systems (EGS) concepts, where heat stored in hot dry rocks is extracted through engineered permeability. The viability of such systems depends strongly on subsurface heat production, thermal conductivity, structural permeability, and fluid circulation pathways. Therefore, understanding the geological and structural framework of granite-dominated terrains is critical in assessing their geothermal potential [3, 11].

In Indonesia, geothermal exploration has predominantly targeted volcanic arcs, while non-volcanic geothermal systems remain underexplored. The Bangka–Belitung region, located off the eastern coast of Sumatra, presents a geological setting distinct from Indonesia's volcanic belts. The region is characterized by extensive Triassic–Jurassic granitic intrusions belonging to the Southeast Asian Tin Belt. These granitic bodies are known for their enrichment in radioactive elements, as evidenced by their association with tin mineralization. Such geological characteristics suggest the potential presence of radiogenic heat sources capable of supporting low- to moderate-enthalpy geothermal systems [12, 13].

The Pelawan area in West Bangka Regency represents one such location where geothermal manifestations have been reported in a non-volcanic setting (Fig. 1). Unlike volcanic geothermal systems, geothermal signatures in Pelawan are not associated with active volcanism but are instead inferred to be structurally controlled and potentially related to granite intrusions. However, the subsurface configuration of the geological formations and the structural framework controlling fluid circulation in this area remain insufficiently understood. A comprehensive subsurface characterization is therefore required to evaluate the geothermal potential and to identify structural features that may facilitate heat and fluid transport.

Structural discontinuities such as faults and fractures play a fundamental role in geothermal systems, particularly in non-volcanic environments. Fault zones can act as conduits for fluid migration, enabling deep circulation of meteoric water that is subsequently heated by radiogenic heat sources [6, 14, 15]. In granite-hosted systems, fault-controlled permeability is often the primary mechanism governing geothermal manifestations. Therefore, identifying the presence, orientation, and spatial distribution of subsurface fault structures is essential for understanding geothermal system dynamics [4, 16].

Geophysical methods provide effective tools for investigating subsurface structures and lithological contrasts without intrusive drilling. Among these methods, gravity surveying is particularly suitable for regional-scale structural analysis and lithological differentiation. The gravity method is based on measuring variations in the Earth's gravitational field caused by density contrasts in subsurface materials. Since granite, sedimentary formations, and alluvial deposits possess distinct density values, gravity anomalies can be used to infer subsurface stratigraphy and structural discontinuities [17, 18].

In geothermal exploration, gravity data have been widely applied to delineate fault zones, intrusive bodies, sediment thickness variations, and basement configurations. Negative or positive Bouguer anomalies often reflect variations in rock density associated with structural features or lithological changes [19–21]. When integrated with geological information, gravity modeling can provide valuable insights into subsurface architecture and potential geothermal heat sources. Furthermore, two-dimensional (2D) and three-dimensional (3D) gravity modeling techniques allow for more detailed interpretation of subsurface geometry and density distribution [1].

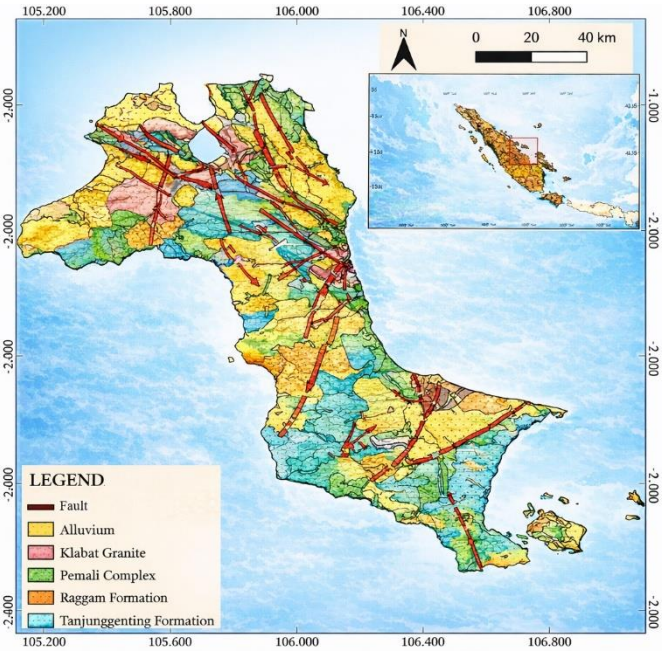


**Fig. 1.** Regional geological in West Bangka Regency, Indonesia.

The availability of satellite-derived gravity datasets, such as those obtained from TOPEX missions, has significantly expanded the accessibility of gravity data for preliminary geothermal assessments. Although satellite gravity data have lower spatial resolution compared to ground-based surveys, they are useful for regional structural mapping and reconnaissance studies, particularly in areas with limited field accessibility. By processing satellite gravity data to obtain Complete Bouguer Anomaly (CBA) values, it is possible to identify density contrasts associated with granitic intrusions and structural features that may control geothermal activity [3, 6, 16].

In the context of Pelawan, the integration of gravity data analysis with existing geological information provides an opportunity to evaluate the structural and lithological framework of a potential radiogenic geothermal system. The geological map of the region indicates the presence of several formations, including Pleistocene alluvium, the Triassic Tanjung Genting Formation, Triassic–Jurassic Klabat Granite, and the Pemali Formation. The Klabat Granite, in particular, is interpreted as a potential radiogenic heat source due to its granitic composition and regional geological setting within the Southeast Asian Tin Belt.

Despite these indications, there remains a lack of detailed subsurface structural interpretation in the Pelawan area. Previous studies have primarily focused on geological mapping and surface manifestations, with limited application of integrated geophysical modeling to characterize subsurface density distribution and fault structures. Consequently, the structural controls and heat source configuration of the Pelawan geothermal system remain inadequately constrained.

This study aims to address this gap by conducting a preliminary subsurface structural analysis of the Pelawan geothermal area using gravity data. Specifically, this research seeks to (1) process and analyze satellite-derived gravity data to obtain Complete Bouguer Anomaly values, (2) construct 2D and 3D gravity models to interpret subsurface density contrasts and lithological boundaries, and (3) identify structural features that may control geothermal manifestations and fluid pathways. By focusing on a granite-dominated non-volcanic terrain, this study contributes to expanding the understanding of radiogenic geothermal systems in Indonesia.

The significance of this research lies in its contribution to diversifying geothermal exploration strategies in Indonesia. As the country continues to expand its renewable energy portfolio, non-volcanic geothermal resources such as radiogenic systems may

represent untapped opportunities. Identifying structurally controlled granite-hosted geothermal systems could open new exploration frontiers beyond traditional volcanic provinces.

In summary, this study provides a gravity-based structural interpretation of a potential radiogenic geothermal system in Pelawan, West Bangka. By integrating geological context with 2D–3D gravity modeling, the research aims to elucidate the subsurface architecture and structural controls governing geothermal manifestations in a non-volcanic granite terrain. The findings are expected to enhance the understanding of radiogenic geothermal systems and support future exploration efforts in similar geological settings.

## 2. Conceptual geological setting

The regional geological framework of Bangka Island is associated with continental crust and forms part of the outer sector of the Sumatra back-arc basin system. Tectonically, Bangka Island is located within the Sunda Shelf (Sundaland Craton), which constitutes a stable fragment of the Eurasian Plate. The island is also part of the Southeast Asian Tin Belt, a major Mesozoic magmatic province characterized by extensive granitic intrusions and significant tin mineralization [6, 14, 15].

The geological evolution of Bangka Island has been strongly influenced by prolonged regional tectonic activity. Plate interactions and tectonic reconfigurations over geological time have resulted in significant rock deformation, producing structural features such as folds, faults, fractures, and regional lineaments. The fault systems identified in the area include reverse faults, normal faults, and strike-slip faults. These structural elements are closely associated with regional folding patterns and play a crucial role in controlling lithological distribution and structural architecture [3, 6, 16].

Lithologically, Bangka Island is dominated by granitic rocks related to Mesozoic magmatic activity. These intrusive igneous rocks represent a key component of the Southeast Asian Tin Belt and are genetically linked to mineralization processes. In addition to the granitic intrusions, sedimentary rock formations were deposited during various tectonic phases, reflecting changes in depositional environments through time [19–21].

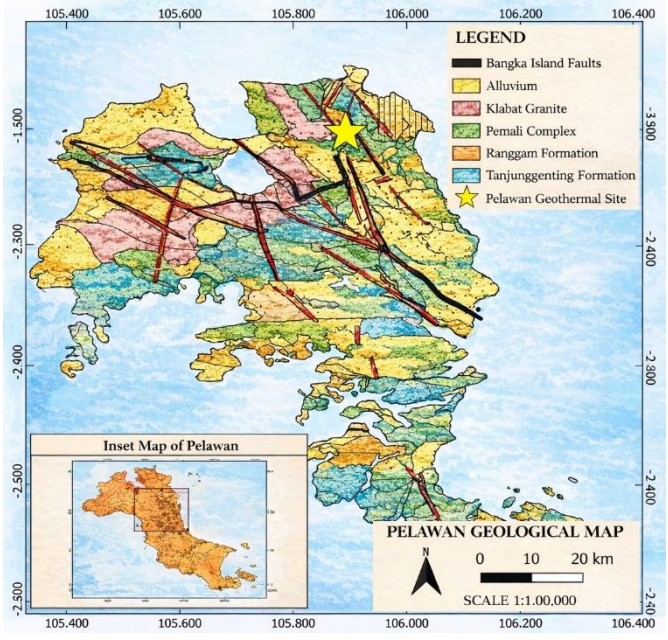


**Fig. 2.** Regional geological in the Pelawan geothermal area, located in West Bangka Regency, Indonesia.

The tectonostratigraphic evolution of Bangka Island began at least as early as the Permian, marked by the formation of the Pemali Complex (CPp). During the Early Triassic, regional subsidence occurred, leading to the deposition of the Tanjung Genting Formation (Trt) in a shallow marine environment. Subsequently, during the Late Triassic to Jurassic, tectonic uplift was accompanied by the intrusion of the Klabat Granite (TrJkg), which represents one of the principal granitic bodies in the region. The Klabat Granite is particularly significant in the context of radiogenic geothermal systems due to its felsic composition and potential enrichment in heat-producing radioactive elements. During the Late Miocene to Early Pleistocene, sedimentation resumed, resulting in the deposition of the Ranggam Formation (TQr). In the Holocene, regional uplift and surface leveling were followed by the accumulation of unconsolidated Quaternary deposits, including fluvial, swamp, and coastal alluvium. These younger deposits generally overlie the older bedrock formations and contribute to the present-day geomorphology of Bangka Island.

Overall, the geological configuration of Bangka Island reflects a complex interaction of magmatic, tectonic, and sedimentary processes. The presence of extensive granitic intrusions, structurally controlled deformation zones, and prolonged tectonic evolution provides a favorable geological setting for the development of structurally controlled radiogenic geothermal systems in non-volcanic environments. Based on the tectonic activity that has occurred, the rocks forming Bangka Island consist of several formations, as illustrated in the geological map of Bangka Island in Fig. 1. The study area location has the same rock formations as shown in Fig. 2. The rocks in the study area are dominated by Klabat granite (TRJkg) and Tanjung Genting granite (TRt) [19–21].

## 3. Method

### 3.1. Study area and data source

The study was conducted in the Pelawan area, West Bangka Regency, Bangka Belitung Islands, Indonesia, located between 1°28′–1°48′ S and 105°13′–106°08′ E (Fig. 1). The research activities were carried out from December 2021 to August 2022. Data processing and analysis were performed at the Geophysics Laboratory, Physics Study Program, Department of Science, Sumatera Institute of Technology. The study area is situated within a granite-dominated non-volcanic terrain associated with the Southeast Asian Tin Belt, making it suitable for investigating radiogenic geothermal potential.

This study utilized secondary gravity and topographic datasets derived from the TOPEX satellite database (http://topex.ucsd.edu/). The acquired data consist of regularly gridded Free-Air Anomaly (FAA) values in ASCII XYZ format, including latitude, longitude, elevation, and gravity anomaly values. Additional geological information was obtained from regional geological maps to support subsurface interpretation. Data processing and modeling were performed using the following software:

- Microsoft Excel (data integration and Bouguer correction calculations)
- Oasis Montaj (terrain correction, spectral analysis, filtering, and 2D modeling)
- Surfer 16 (data gridding and visualization)
- Global Mapper (topographic data processing)
- QGIS 3.16 (geospatial data integration)
- Grablox 1.6e (3D gravity modeling)
- Bloxer 1.6e (3D visualization and interpretation)
- Google Earth Pro (geographic reference validation)

### 3.2. Gravity data processing

Initial data processing was conducted in Microsoft Excel 2019. The FAA and elevation datasets were combined into a single database for correction calculations. The Complete Bouguer Anomaly (CBA) was calculated through the following steps:

1. Free-air correction (already included in FAA data).
2. Bouguer correction using an estimated average rock density.

3. Terrain correction to remove topographic effects.

The Bouguer correction was applied to obtain the Simple Bouguer Anomaly (SBA) [14, 22, 23] using equation (1).

$$\Delta g_B = \Delta g_{FA} - (0.04193\rho h) \quad \ldots (1)$$

where $\rho$ is the Bouguer density (g/cm³) and $h$ is elevation (m).

Optimal Bouguer density was determined through correlation analysis between gravity anomaly and elevation values. The density value minimizing correlation was selected as the representative surface density. Terrain correction was performed in Oasis Montaj using SRTM-derived elevation data. The terrain correction values were then added to the SBA to obtain the (CBA) was calculated as equation (2).

$$CBA = FAA - Bouguer\ Correction + Terrain\ Correction \quad \ldots (2)$$

The corrected dataset was subsequently converted into UTM Zone 48S coordinates for spatial analysis.

### 3.3. Spectral analysis and regional–residual separation

Spectral analysis was performed in Oasis Montaj to estimate the average depth of gravity anomaly sources and to separate regional and residual components. The Fourier transform was applied to the CBA dataset, converting spatial-domain gravity data into the frequency (wavenumber) domain in equation (3).

$$F(k) = \int_{-\infty}^{\infty} f(x) e^{-ikx} dx \quad \ldots (3)$$

The logarithmic power spectrum was plotted as log amplitude versus wavenumber. The slope of linear segments was used to estimate source depth, where steeper slopes correspond to deeper sources and gentler slopes indicate shallower structures. Regional and residual anomalies were separated using frequency-domain filtering:

- Low-pass filter → isolates deep regional anomalies
- Band-pass filter → highlights shallow residual anomalies

Residual anomalies are interpreted to represent shallow density contrasts related to structural features and geothermal circulation pathways.

### 3.4. Two and three-dimensional forward modeling

Two-dimensional forward modeling was conducted along selected profiles crossing significant gravity anomalies. The objective was to estimate subsurface geometry and density distribution consistent with observed gravity responses. Modeling was performed using Oasis Montaj, integrating geological constraints. A trial-and-error forward modeling approach was applied until the misfit between observed and calculated anomalies was minimized (error <5%). The minimum and maximum density values obtained from 2D modeling were used as constraints for subsequent 3D inversion modeling. Three-dimensional gravity modeling was performed using Grablox 1.6e, with visualization in Bloxer 1.6e. The workflow consisted of:

1. Initial Forward Modeling

   A block model representing the study area was constructed based on gridded Complete Bouguer Anomaly data. Major and minor blocks were defined according to spatial resolution and area extent.

2. Density Parameter Assignment

   Density values derived from 2D modeling were assigned as initial constraints.

3. Inverse Modeling

   An iterative inversion procedure was applied to adjust density distribution and geometry to minimize misfit between observed and calculated gravity anomalies. Optimization stages included:

   - Base model adjustment
   - Density optimization
   - Occam density smoothing
   - Elevation adjustment
   - Occam height smoothing

The inversion process aimed to reduce residual error and obtain a geologically reasonable subsurface density model.

### 3.5. Data interpretation

Interpretation was conducted qualitatively and quantitatively. For the qualitative interpretation, gravity anomaly maps (Complete Bouguer, regional, and residual) were analyzed to identify patterns associated with density contrasts. High gravity anomalies were interpreted as potential granitoid intrusions or basement highs, whereas low residual anomalies were interpreted as fractured or altered zones possibly associated with geothermal fluid pathways.

While quantitative interpretation, the cross-sectional models from 2D forward modeling and volumetric density distributions from 3D inversion were integrated with geological maps. Density contrasts were correlated with lithological units and structural features, particularly fault systems that may act as geothermal conduits. The final interpretation focuses on identifying:

- Potential granite heat sources
- Structural controls (faults/fractures)
- Zones of reduced density indicative of hydrothermal alteration

## 4. Results and discussion

### 4.1. Complete bouguer anomaly (CBA) map

Qualitative interpretation was carried out by analyzing the spatial distribution and pattern of the Complete Bouguer Anomaly (CBA) and correlating it with regional geological settings and previous studies. This approach allows for preliminary identification of subsurface structural configurations and lithological variations within the study area. The CBA map (Fig. 3) was generated using an average density of 2.67 g/cm³. The results indicate that anomaly values within the study area range from 10.7 mGal to 40.8 mGal (Figure 4.1). High gravity anomalies, ranging from 30.9 to 40.8 mGal, are interpreted to be associated with dense intrusive bodies, particularly the Klabat Granite. These high-density zones likely represent granitic intrusions at shallow to intermediate depths, which are consistent with the regional geological framework.

In contrast, low gravity anomalies, ranging from 10.7 to 29.5 mGal and represented by blue to light-blue colors on the anomaly map, are interpreted as less dense sedimentary deposits, primarily alluvial formations. These units are characterized by lower density values of approximately 1.8–1.9 g/cm³. The distribution of low-anomaly zones generally corresponds to surface sedimentary cover and topographically lower areas. The contrast between high- and low-anomaly zones reflects significant subsurface density variations, which are interpreted to be controlled by the distribution of granitic basement rocks and overlying sedimentary formations. These density contrasts provide important insights into the structural framework of the Pelawan geothermal system and suggest the presence of granite-dominated heat sources beneath relatively low-density sedimentary cover [24].

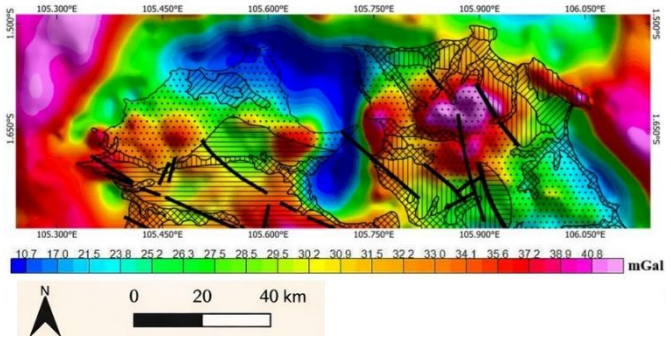


**Fig. 3.** Complete bouguer anomaly (CBA) map in the Pelawan geothermal area, located in West Bangka Regency, Indonesia.

### 4.2. Spectral analysis and depth estimation

The estimation of regional and residual anomaly depths was

conducted through spectral analysis by examining the relationship between the logarithm of amplitude and the wavenumber (k). In this approach, the slope of the linear segments in the amplitude–wavenumber spectrum is directly related to the depth of the corresponding anomaly sources. Steeper slopes indicate deeper sources (regional anomalies), whereas gentler slopes correspond to shallower sources (residual anomalies). As illustrated in Fig. 4, the radially averaged power spectrum reveals three distinct segments characterized by different gradient values. These segments represent (1) deep regional sources, (2) intermediate to shallow residual sources, and (3) high-frequency noise components. The separation of these spectral domains enables the determination of cutoff wavenumbers used to distinguish between regional and residual anomalies.

The regional component is associated with long-wavelength anomalies generated by deeper density contrasts, while the residual component reflects short-wavelength anomalies related to shallow subsurface structures. The identification of these three spectral domains provides a quantitative basis for subsequent anomaly filtering and structural interpretation. [20, 21, 25].

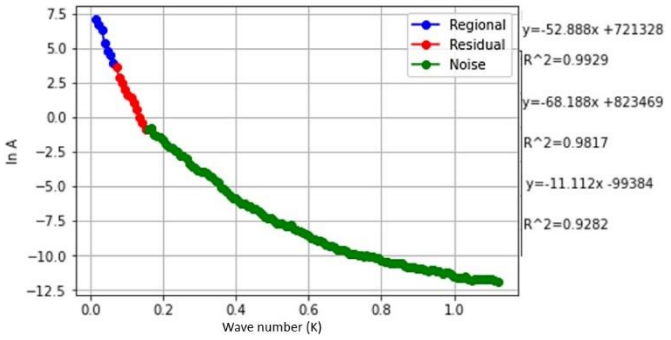


**Fig. 4.** Spectral analysis.

The spectrum curve reveals three distinct segments corresponding to three different discontinuity levels, each representing anomaly sources at different depths. The boundaries between these segments were determined based on the coefficient of determination ($R^2$), which serves as a control parameter describing the linear relationship between the independent variable (wavenumber, k) and the dependent variable (logarithm of amplitude, ln A). The identification of these linear segments allows for the separation of the anomaly into three domains: regional, residual, and noise components.

The regional anomaly zone is defined by a cutoff wavenumber of 0.09929 (1/km), representing long-wavelength components associated with deeper sources. The residual anomaly zone is separated by a cutoff wavenumber of 0.09817 (1/km), corresponding to intermediate to shallow sources. Meanwhile, the high-frequency noise component is characterized by a cutoff wavenumber of 0.09282 (1/km). These cutoff wavenumbers were used to define spectral windows for depth estimation based on the slope of each linear segment in the power spectrum (Fig. 5).

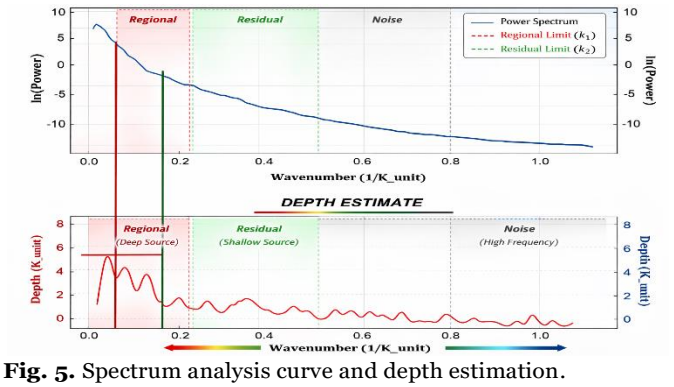


**Fig. 5.** Spectrum analysis curve and depth estimation.

Depth estimation was conducted by projecting the linear slopes onto the depth–wavenumber relationship, where vertical lines indicate cutoff wavenumbers and horizontal lines represent the corresponding estimated depths. Based on the spectral analysis results, the estimated depth of the regional anomaly source is approximately 6.6 km, indicating deep-seated density contrasts likely associated with basement structures. In contrast, the residual anomaly source is estimated at approximately 2.5 km depth, suggesting shallower structural features that may be related to fault systems or intrusive bodies controlling the geothermal system. These results provide a quantitative basis for distinguishing deep and shallow density sources and serve as an essential input for subsequent 2D and 3D gravity modeling.

### 4.3. *Separation of regional and residual anomalies*

The separation of regional and residual anomalies was performed using low-pass and band-pass filtering techniques. This procedure aims to distinguish between deep-seated anomaly sources (regional component) and shallow anomaly sources (residual component). The band-pass filter was applied to isolate the residual anomaly by retaining a specific range of wavenumbers associated with intermediate to high frequencies, while attenuating wavelengths outside the selected range. This approach enhances short-wavelength features that are typically related to shallow subsurface structures such as faults, fractures, and near-surface lithological contrasts.

In contrast, the low-pass filter was used to extract the regional anomaly component by preserving low-wavenumber (long-wavelength) signals and suppressing high-wavenumber components. The regional anomaly represents deep density contrasts, commonly associated with basement structures or large-scale lithological variations. The application of these filtering techniques resulted in two separate anomaly maps: the regional anomaly map (Fig. 6), which reflects deep structural features, and the residual anomaly map (Fig. 7), which highlights shallow geological structures. These filtered maps provide a clearer basis for structural interpretation and subsequent gravity modeling [16, 26, 27].

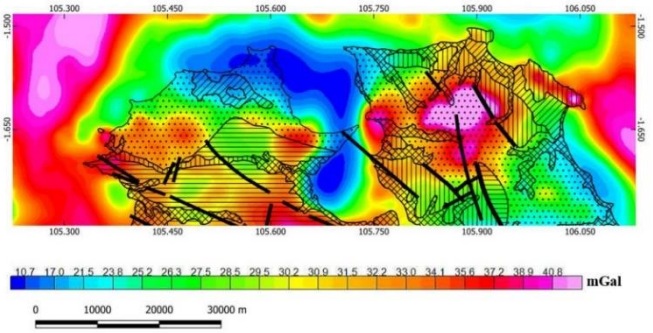


**Fig. 6.** Regional gravity anomaly map of the Pelawan geothermal area, located in West Bangka Regency, Indonesia.

Based on the regional anomaly map (Fig. 6), the gravity response can be classified into two principal patterns: high-anomaly zones and low-anomaly zones. The high-anomaly values range from 31.5 to 40.8 mGal and are represented by orange to pink colors, whereas the low-anomaly values range from 10.7 to 30.9 mGal and are depicted in blue to light-blue tones. Geologically, the study area comprises the Tanjung Genting Formation, Klabat Granite, and the Pemali Complex, with the granitic units interpreted to extend to greater depths compared to the surrounding formations. The high regional gravity anomalies are interpreted as dense granitic bodies associated with the Klabat Granite formation. The dominance of high-anomaly zones in Fig. 6 indicates that the subsurface of the study area is largely controlled by extensive granite intrusions at depth [16, 26, 27].

In contrast, the low-anomaly zones are interpreted to correspond to less dense sedimentary rocks, particularly sandstone units belonging to the Tanjung Genting Formation. The lower density of these sedimentary formations results in reduced gravity values compared to the granitic

basement. The contrast between high and low regional anomalies reflects significant deep density variations and suggests that the subsurface structure of the Pelawan area is predominantly influenced by granite-dominated basement rocks, which are likely to play an important role in the development of the radiogenic geothermal system.

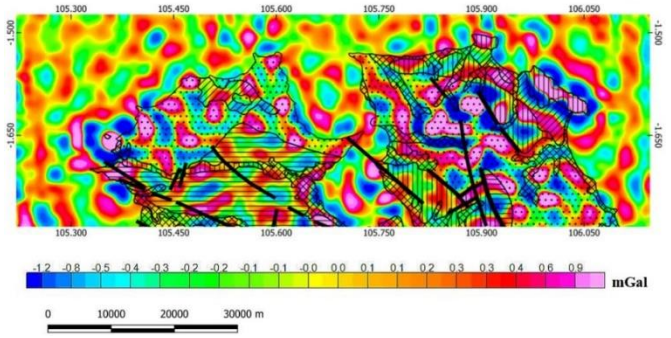


**Fig. 7.** Residual gravity anomaly map.

The residual anomaly map reveals three distinct anomaly patterns: low, moderate, and high anomaly zones. The low residual anomalies range from −1.2 mGal to −0.4 mGal and are represented by blue to light-blue colors. Moderate anomalies range from −0.3 mGal to 0.0 mGal and are depicted in green to orange tones. High residual anomalies range from 0.1 mGal to 0.9 mGal and are illustrated in red to pink colors. The low residual anomaly zones are interpreted as low-density near-surface deposits, including alluvial sediments, swamp deposits, and quartz sand accumulations. These materials are characterized by relatively low bulk density and correspond to shallow sedimentary cover [20, 21, 25].

In contrast, the high residual anomaly zones are interpreted as shallow intrusive granitic bodies that locally penetrate overlying sedimentary formations. These intrusions are inferred to cut through lithologies such as sandstone, metamorphosed sandstone, clayey sandstone, and claystone with limestone lenses, which are components of the Triassic Tanjung Genting Formation. The spatial distribution of high residual anomalies suggests the presence of shallow granite intrusions or structural uplift zones, which may play a significant role in controlling the subsurface architecture. These shallow density contrasts are particularly important in the context of radiogenic geothermal systems, as granitic intrusions may act as heat-producing bodies beneath the sedimentary cover [16, 26, 27].

### *4.4. 2D gravity anomaly modeling*

Quantitative interpretation was conducted through 2D gravity modeling by analyzing anomaly patterns along selected cross-sectional profiles, as shown in Fig. 8. The modeling was based on the Complete Bouguer Anomaly (CBA) map integrated with the regional geological map of the study area. The interpretation incorporated results from the previous qualitative analysis to constrain anomaly boundaries and to estimate the geometry of subsurface structures along each profile. Two profiles, A–A′ and B–B′, were constructed to intersect the Pelawan geothermal area and surrounding fault structures. These profiles were specifically designed to cross both high- and low-anomaly zones to capture the lateral and vertical density variations associated with the geothermal system.

Profile A–A′ intersects several high- and low-anomaly segments, with gravity values ranging from a maximum of 40.8 mGal to a minimum of 10.7 mGal. The resulting 2D model for profile A–A′ (Fig. 9) indicates a maximum modeled depth of approximately 7.69 km along a profile length of 40 km. The subsurface configuration suggests significant density contrasts corresponding to granitic basement rocks and overlying sedimentary formations. Fault structures identified along the profile are interpreted as structural controls of the radiogenic geothermal system. These fault zones likely act as conduits that connect deep-seated granite-derived heat sources with shallow groundwater systems, facilitating fluid circulation and geothermal manifestation at the surface. The integration of gravity modeling and geological constraints thus provides a robust framework for identifying structural pathways and potential heat-source geometry in the Pelawan geothermal area.

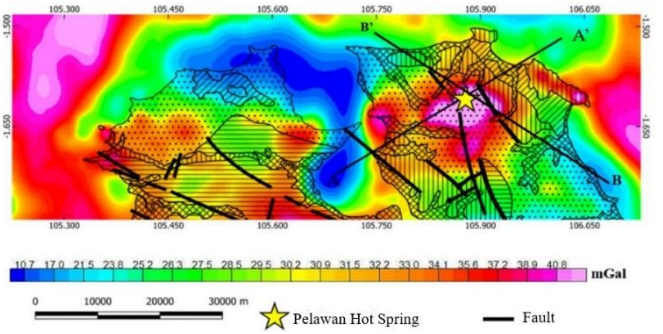


**Fig. 8.** Integrated geological and Complete Bouguer Anomaly (CBA) map of Pelawan geothermal area, located in West Bangka Regency, Indonesia.

Based on Fig. 9, the modeling error obtained for profile A–A′ is 4.91%, indicating a good agreement between the observed and calculated gravity responses. The 2D modeling results reveal a subsurface stratigraphy composed of the Alluvium Formation, Ranggam Formation, Tanjung Genting Formation, and the Pemali Complex. The uppermost layer consists of the Alluvium Formation, characterized by a density of approximately 1.90 g/cm³. This unit comprises unconsolidated materials such as boulders, gravel, sand, clay, and peat deposits of Holocene age. As the youngest geological formation in the area, the Alluvium Formation represents recent surface deposits widely distributed across Bangka Island.

Beneath the alluvial deposits lies the Ranggam Formation, with an estimated density of 2.47 g/cm³. This formation is interpreted to be of Late Miocene to Pliocene age and consists of interbedded sandstone and tuffaceous claystone with thin siltstone intercalations. The lithological composition suggests a transitional sedimentary environment. The Tanjung Genting Formation forms the next stratigraphic layer, with a density of approximately 2.50 g/cm³. This Triassic-aged formation consists predominantly of sandstone and claystone and is significantly older than the overlying alluvial deposits. According to the regional geological map, this formation is affected by fault structures generated by tectonic activity, which may play an important role in controlling subsurface fluid migration.

At greater depths, the modeling results indicate the presence of the Pemali Complex, characterized by a higher density of approximately 2.69 g/cm³. The relatively high density suggests more consolidated or metamorphosed lithologies compared to the overlying sedimentary formations. This unit likely represents part of the deeper basement structure underlying the study area. The density contrasts between these formations provide important constraints for understanding the structural framework and subsurface architecture associated with the Pelawan geothermal system.

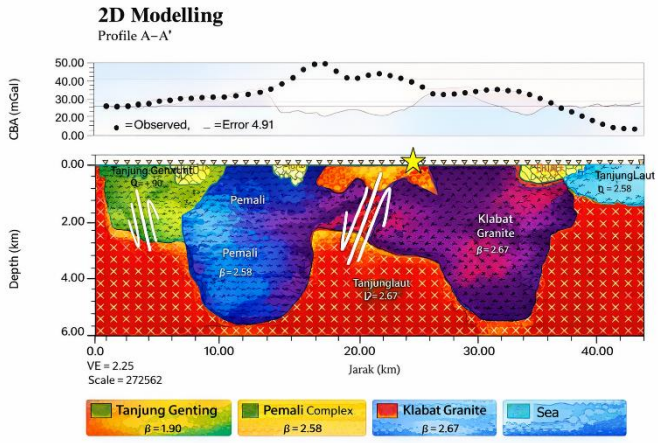


**Fig. 9.** Results of 2D modelling of section A-A'

The Pemali Complex, dating from the Permian period, is the oldest formation and is therefore identified as basement rock. According to geological maps, within the Pemali Formation there are faults in the geothermal area, specifically granite intrusions resulting from fault structures.

Profile B–B′ was constructed to evaluate whether the identified fault structures contribute significantly as controlling elements of the geothermal system. Based on Fig. 10, the modeling error obtained for profile B–B′ is 4.81%, indicating a satisfactory fit between the observed and calculated gravity anomalies. The B–B′ profile extends approximately 90 km with a maximum modeled depth of 7.69 km. Along this profile, gravity anomaly values range from 17.0 to 38.9 mGal, forming a distinct anomaly depression as illustrated in Fig. 8. This anomaly configuration suggests significant lateral and vertical density contrasts within the subsurface.

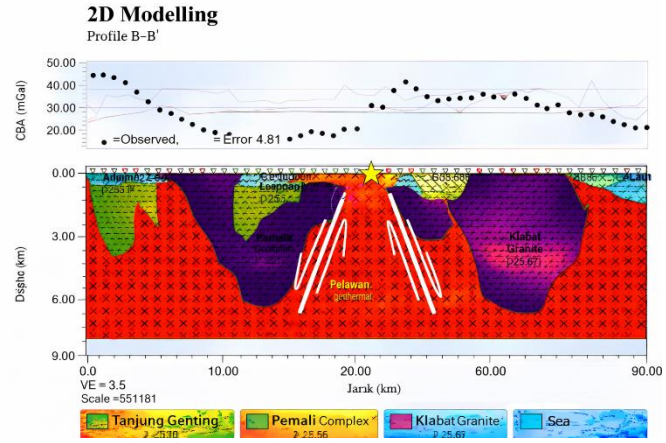


**Fig. 10.** Results of 2D modelling of section B-B'

At the surface, the profile intersects several geological formations, including the Tanjung Genting Formation, Alluvium Formation, Ranggam Formation, and Klabat Granite. The deeper part of the model is predominantly composed of the Klabat Granite, characterized by a density of approximately 2.58 g/cm³. The extensive distribution of this granitic body at depth supports its interpretation as the principal basement unit beneath the study area.

The Klabat Granite is interpreted as the primary radiogenic heat source in the Pelawan geothermal system. Radiogenic heat generation in granitic rocks is mainly associated with the radioactive decay of heat-producing elements such as uranium (U), thorium (Th), and potassium (K). These elements are commonly enriched in felsic intrusive rocks, particularly granites, making them significant contributors to crustal heat production. The presence of granite-dominated basement rocks therefore provides strong geological support for the development of a radiogenic geothermal system in Bangka Island.

Furthermore, the modeled fault structures along profile B–B′ likely act as permeable pathways that facilitate the upward migration of heat and fluids from the granite basement to the surface, thereby enhancing geothermal manifestations in the Pelawan area.

### 4.5. *Three-dimensional forward and inverse modeling*

The three-dimensional (3D) gravity modeling was conducted in two principal stages: forward modeling and inverse modeling. The forward modeling stage was designed to construct an initial subsurface model representing the geometry and physical properties of the study area. The study domain extends approximately 101.98 km along the x-axis and 35.03 km along the y-axis. This domain was discretized into 20 × 20 horizontal blocks, producing 400 minor blocks per layer. Vertically, the model extends to a depth of 7.69 km and was subdivided into eight layers, resulting in a total of 3,200 volumetric cells. This discretization scheme was selected to ensure an appropriate balance between spatial resolution and computational stability during inversion.

he initial density range was constrained between 1.0 and 2.8 g/cm³, based on the average density of continental crustal rocks and geological information from Bangka Island. The upper density limit (2.8 g/cm³) is consistent with previous 2D gravity modeling results in the same region, thereby maintaining methodological consistency and reducing model ambiguity [16].

### 4.6. *Inversion strategy and model optimization*

The inversion process was carried out using the Grablox software package, with sequential optimization of several key parameters: (1). Base level correction; (2). Density contrast optimization; (3). Occam regularization for density (Occam d); (4). Layer elevation optimization; (5). Occam regularization for elevation (Occam h).

The primary objective of the inversion procedure was to estimate subsurface physical parameters that are not directly observable, by minimizing the misfit between observed Bouguer gravity anomalies and calculated model responses. The base level optimization yielded a very low residual error, indicating that systematic bias in the gravity anomaly baseline was effectively corrected. This step is critical to prevent propagation of systematic errors into subsequent inversion stages.

Density optimization resulted in a relative error of 0.3767%, demonstrating excellent agreement between observed and modeled gravity data. The modeled anomaly values range from −14 mGal to 57 mGal, consistent with the measured complete Bouguer anomaly across the study area. To avoid overfitting and to obtain a geologically realistic solution, Occam regularization was applied to the density parameter (Occam d). This approach favors a minimum-structure solution, ensuring smooth spatial variations in density while preserving data fidelity.

Subsequently, layer elevation optimization was performed to refine the vertical geometry and thickness of subsurface layers. Because gravity inversion is inherently non-unique and sensitive to depth variations, additional Occam regularization was applied to elevation parameters (Occam h). The final Occam h optimization produced a residual error of 0.4546%, with anomaly values ranging from 5 to 57 mGal. Although the misfit slightly increased compared to density-only optimization, the integrated model provides improved geological plausibility and structural coherence. Overall, the final model achieves a data misfit below 1%, indicating a high level of reliability in reproducing observed gravity responses [16].

### 4.7. *Three-dimensional subsurface structure of the Pelawan geothermal area*

The final inversion model was visualized using Bloxer 1.6e to generate a three-dimensional representation of subsurface structures beneath the Pelawan geothermal area. The model consists of eight layers extending to a maximum depth of 7.69 km. Density values across the model vary between 1.0 and 2.8 g/cm³, represented by a color scale indicating density contrasts between adjacent blocks. Significant lateral and vertical density heterogeneities are observed within the model. Zones characterized by relatively low densities (approximately 1.0–2.2 g/cm³) are interpreted as altered rocks, weathered formations, sedimentary units, or fractured zones potentially saturated with hydrothermal fluids. These features are consistent with typical density reductions associated with hydrothermal alteration processes.

Conversely, higher-density zones (≥2.6 g/cm³) are interpreted as compact crystalline basement rocks or intrusive igneous bodies. Such high-density anomalies may indicate magmatic intrusions that could serve as a heat source for the geothermal system. Spatially, the modeled Bouguer anomaly pattern correlates with known geothermal manifestations in the Pelawan area. Intermediate-depth density contrasts may delineate structural boundaries, fault-controlled permeability zones, or potential reservoir compartments within the hydrothermal system. The 3D model therefore provides important structural insights into the subsurface configuration controlling geothermal activity in the region (Fig. 11).

The application of Occam regularization ensures that the resulting model is stable, minimally parameterized, and geologically consistent. The low residual error (<1%) indicates excellent agreement between observed and calculated gravity data. However, gravity inversion remains inherently non-unique. Multiple subsurface configurations

may produce similar gravity responses. Therefore, the geological interpretation presented here should be integrated with independent datasets such as geological mapping, geochemical analysis, magnetotelluric data, or seismic investigations to further reduce ambiguity. Despite these limitations, the 3D gravity inversion model provides a robust first-order characterization of subsurface density distribution in the Pelawan geothermal area (Fig. 11). The identified density contrasts suggest structural controls and potential reservoir zones that are relevant for future geothermal exploration and development.

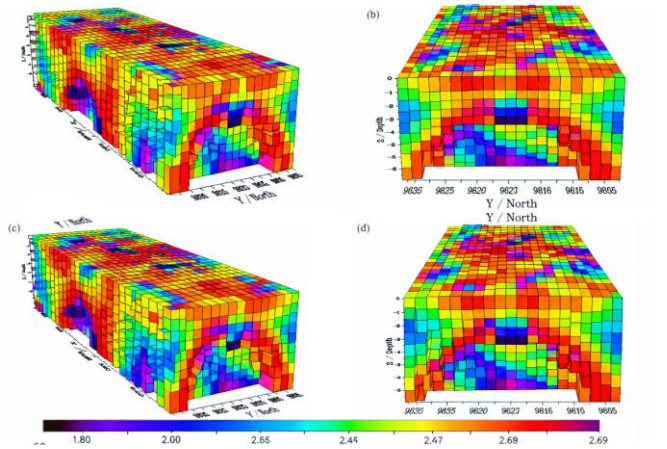


**Fig. 11.** 3D subsurface model of the Pemali geothermal area.

### *4.8. Interpretation of the Pemali geothermal system*

The interpretation was conducted through an integrated analysis of the 2D cross-section along profile A–A', the conceptual radiogenic geothermal system model of the study area, and the final 3D inversion model. In a hydrothermal reservoir system sourced from meteoric water, geothermal fluids originate primarily from infiltrating rainfall. Precipitation percolates downward through fractures and permeable rock formations, where it accumulates within reservoir units. When these infiltrating fluids encounter a subsurface heat source, thermal energy is transferred to the fluid through both conduction (within solid rocks) and convection (within the circulating fluids).

Convective heat transfer is driven by buoyancy forces, as described in geothermal fluid dynamics studies. Although gravitational forces initially cause meteoric water to migrate downward, interaction with a heat source increases fluid temperature, thereby reducing its density. The resulting buoyancy contrast induces upward migration of heated fluids, establishing a convective circulation system characteristic of hydrothermal reservoirs.

The 3D inversion results indicate the presence of a granitic intrusion penetrating sandstone formations within the study area. High-density zones (represented in red) are interpreted as granitic rocks belonging to the Klabat Granite Formation. These granitic bodies exhibit locally interbedded or adjacent zones of relatively lower density (represented in yellow), which are interpreted as sandstone units associated with the Tanjung Genting Formation. The each layer of the 3D model, corresponding to the deepest section (~7.69 km), is dominated by high-density values. These high-density anomalies are interpreted as extensive granitic basement rocks underlying Bangka Island. This interpretation is consistent with regional geological studies indicating that Bangka Island is predominantly composed of granitic intrusions.

Importantly, the granitic rocks in Bangka Island are known to contain radiogenic elements such as uranium (U), thorium (Th), and potassium (K). The radioactive decay of these elements generates internal heat over geological timescales. This radiogenic heat production may contribute significantly to the thermal regime of the subsurface, supporting the development of a radiogenic geothermal system rather than a magmatically driven volcanic system.

The integration of density contrasts, geological information, and geothermal conceptual modeling suggests that the Pemali geothermal system (Fig. 12) is likely controlled by:

- Radiogenic heat production from granitic basement rocks,
- Structural permeability provided by fractures and faults, and
- Meteoric water recharge driving hydrothermal convection.

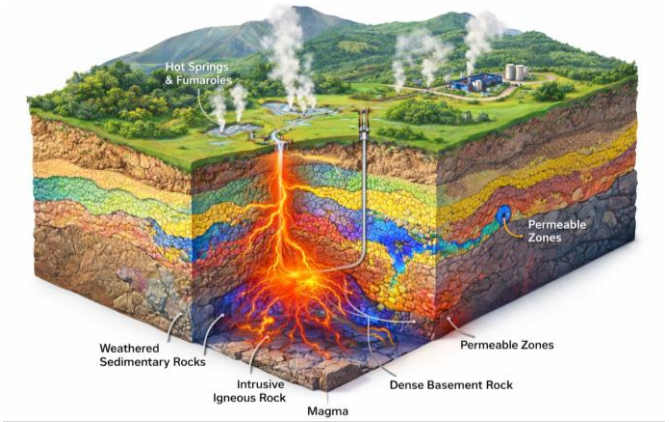


**Fig. 12.** Illustration of 3D subsurface model of the Pemali geothermal system. Deep granitic bodies act as radiogenic heat sources, while folded sedimentary formations serve as permeable reservoirs.

This interpretation supports a non-volcanic, granite-hosted geothermal system model, which is increasingly recognized in several regions worldwide as a viable geothermal resource type. Overall, the integration of density modeling and structural interpretation confirms that the Pemali geothermal system represents a granite-dominated, fault-controlled, low-temperature geothermal system, where radiogenic heat production within deep intrusive bodies plays a key role in sustaining thermal anomalies. [28, 29].

## 5. Conclusion

Based on the gravity investigation conducted in the Pelawan geothermal area, the complete Bouguer anomaly (CBA) map calculated using an average density of 2.67 g/cm³ reveals distinct anomaly contrasts across the study region. High gravity anomalies range between 30.9 and 40.8 mGal, while low anomalies range from 10.7 to 29.5 mGal. These variations indicate significant subsurface density heterogeneity, which is closely related to differences in lithology and structural features. Integrated 2D and 3D subsurface modeling to a depth of approximately 7.69 km demonstrates that the Pelawan geothermal system is structurally controlled and lithologically dominated by granitic basement rocks. The complete Bouguer anomaly inversion results suggest that the subsurface stratigraphy consists of several major formations. The uppermost layer corresponds to Pleistocene alluvial deposits with densities ranging from 1.8 to 1.9 g/cm³, underlain by the Triassic Tanjung Genting Formation with an average density of approximately 2.1 g/cm³. At greater depths, the subsurface is dominated by the Triassic–Jurassic Klabat Granite Formation, characterized by higher densities around 2.58 g/cm³, and the Pemali Formation acting as the basement rock with an average density of approximately 2.6 g/cm³. The predominance of granitic formations, combined with identified fault structures, supports the interpretation that the Pelawan geothermal system is associated with a granite-hosted geothermal setting. Density contrasts identified in the 3D model highlight structural discontinuities that may serve as fluid pathways and potential reservoir zones.

## CRediT authorship contribution statement

**Meita Tasya Setiawan:** Writing – review & editing, Writing – original draft, Supervision, Software, Resources, Methodology, Investigation, Formal analysis, Data curation. **Mikael Syväjärvi:** Writing – review & editing.

## Declaration of Competing Interest

The authors declare that they have no known competing financial interests or personal relationships that could have appeared to influence the work reported in this paper.

## Data availability

Data will be made available on request.

## Acknowledgment

The authors would like to express their sincere gratitude to all institutions and individuals who contributed to this research. We acknowledge the support provided by the relevant geological and geophysical agencies for access to gravity data and regional geological information of the Pelawan–Pemali area.

## References

1. Hosono, T., Hartmann, J., Louvat, P., Amann, T., Washington, K. E., West, A. J., Okamura, K., Böttcher, M. E., and Gaillardet, J. (2018). Earthquake-Induced Structural Deformations Enhance Long-Term Solute Fluxes from Active Volcanic Systems, *Scientific Reports*, Vol. 8, No. 1, 1–12. doi:10.1038/s41598-018-32735-1.
2. Zhang, Z., Yao, H., Wang, W., and Liu, C. (2021). 3-D Crustal Azimuthal Anisotropy Reveals Multi-Stage Deformation Processes of the Sichuan Basin and Its Adjacent Journal of Geophysical Research : Solid Earth, *Journal of Geophysical Research: Solid Earth*, Vol. 127, No. e2021JB023289, 1–17. doi:10.1029/2021JB023289.
3. Liu, S., Suardi, I., Xu, X., Yang, S., and Tong, P. (2021). The Geometry of the Subducted Slab Beneath Sumatra Revealed by Regional and Teleseismic Traveltime Tomography, *Journal of Geophysical Research: Solid Earth*, Vol. 126, No. 1, 1–29. doi:10.1029/2020JB020169.
4. Dewi, K. C. S., Siregar, R. N., Ningati, T. I., Pulungan, Z. N., Indriyawati, A., and Takahashi, H. (2025). Analysis of Subsurface Faults Using 3D Gravity Method Based On Satellite Image Data : Insights into Indo-Australian and Eurasian Plate Subduction in the Formation of An Accretionary Prism, *International Journal of Hydrological and Environmental for Sustainability*, Vol. 4, No. 3, 135–148.
5. Hariyono, E., and S, L. (2018). The Characteristics of Volcanic Eruption in Indonesia, *Volcanoes - Geological and Geophysical Setting, Theoretical Aspects and Numerical Modeling, Applications to Industry and Their Impact on the Human Health*, No. July. doi:10.5772/intechopen.71449.
6. McCaffrey, R. (2009). The Tectonic Framework of the Sumatran Subduction Zone, *Annual Review of Earth and Planetary Sciences*, Vol. 37, 345–366. doi:10.1146/annurev.earth.031208.100212.
7. Hristov, V., Stoyanov, N., Valtchev, S., Kolev, S., and Benderev, A. (2019). Utilization of Low Enthalpy Geothermal Energy in Bulgaria, *IOP Conference Series: Earth and Environmental Science*, Vol. 249, No. 1. doi:10.1088/1755-1315/249/1/012035.
8. Taruna, R. M., and Banyunegoro, V. H. (2018). Earthquake Relocation Using Double Difference Method for 2D Modelling of Subducting Slab and Back Arc Thrust in West Nusa Tenggara, *Jurnal Penelitian Fisika Dan Aplikasinya (JPFA)*, Vol. 8, No. 2, 132. doi:10.26740/jpfa.v8n2.p132-143.
9. Collings, R., Lange, D., Rietbrock, A., Tilmann, F., Natawidjaja, D., Suwargadi, B., Miller, M., and Saul, J. (2012). Structure and Seismogenic Properties of the Mentawai Segment of the Sumatra Subduction Zone Revealed by Local Earthquake Traveltime Tomography, *Journal of Geophysical Research*, Vol. 117, 1–23. doi:10.1029/2011JB008469.
10. Jihad, A., Muksin, U., Syamsidik, and Ramli, M. (2021). Earthquake Relocation to Understand the Megathrust Segments along the Sumatran Subduction Zone, *IOP Conference Series: Earth and Environmental Science*, Vol. 630, 012002. doi:10.1088/1755-1315/630/1/012002.
11. Xu, J., and Kono, Y. (2002). Geometry of Slab, Intraslab Stress Field and Its Tectonic Implication in the Nankai Trough, Japan, *Earth, Planets and Space*, Vol. 54, No. 7, 733–742. doi:10.1186/BF03351726.
12. Kusuhara, F., Kazahaya, K., Morikawa, N., Yasuhara, M., Tanaka, H., Takahashi, M., and Tosaki, Y. (2020). Original Composition and Formation Process of Slab-Derived Deep Brine from Kashio Mineral Spring in Central Japan, *Earth, Planets and Space*, Vol. 72, No. 1. doi:10.1186/s40623-020-01225-y.
13. Malod, J. A., Karta, K., Beslier, M. O., and Zen, M. T. (1995). From Normal to Oblique Subduction: Tectonic Relationships between Java and Sumatra, *Journal of Southeast Asian Earth Sciences*, Vol. 12, Nos. 1–2, 85–93. doi:10.1016/0743-9547(95)00023-2.
14. Li, C. F. (2011). An Integrated Geodynamic Model of the Nankai Subduction Zone and Neighboring Regions from Geophysical Inversion and Modeling, *Journal of Geodynamics*, Vol. 51, No. 1, 64–80. doi:10.1016/j.jog.2010.08.003.
15. Stern, R. J. (2002). Subduction Zones, *Reviews of Geophysics*, Vol. 40, No. 4, 3-1-3–38. doi:10.1029/2001RG000108.
16. Utama, H. W., Mulyasari, R., and Said, Y. M. (2021). Geothermal Potential on Sumatra Fault System To Sustainable Geotourism in West Sumatra, *JGE (Jurnal Geofisika Eksplorasi)*, Vol. 7, No. 2, 126–137. doi:10.23960/jge.v7i2.128.
17. Tabei, T., Hashimoto, M., Miyazaki, S., Hirahara, K., Kimata, F., Matsushima, T., Tanaka, T., Eguchi, Y., Takaya, T., Hoso, Y., Ohya, F., and Kato, T. (2002). Subsurface Structure and Faulting of the Median Tectonic Line, Southwest Japan Inferred from GPS Velocity Field, *Earth, Planets and Space*, Vol. 54, No. 11, 1065–1070. doi:10.1186/BF03353303.
18. Tongkul, F. (2017). Active Tectonics in Sabah – Seismicity and Active Faults, *Bulletin of the Geological Society of Malaysia*, Vol. 64, No. December, 27–36. doi:10.7186/bgsm64201703.
19. Maryanto, S. (2017). Geo Techno Park Potential at Arjuno-Welirang Volcano Hosted Geothermal Area, Batu, East Java, Indonesia (Multi Geophysical Approach), *AIP Conference Proceedings*, Vol. 1908, No. 2017. doi:10.1063/1.5012712.
20. Sujitapan, C., Kendall, J. M., Chambers, J. E., and Yordkayhun, S. (2024). Landslide Assessment through Integrated Geoelectrical and Seismic Methods: A Case Study in Thungsong Site, Southern Thailand, *Heliyon*, Vol. 10, No. 2. doi:10.1016/j.heliyon.2024.e24660.
21. Chambers, J., Holmes, J., Whiteley, J., Boyd, J., Meldrum, P., Wilkinson, P., Kuras, O., Swift, R., Harrison, H., Glendinning, S., Stirling, R., Huntley, D., Slater, N., and Donohue, S. (2022). Long-Term Geoelectrical Monitoring of Landslides in Natural and Engineered Slopes, *Leading Edge*, Vol. 41, No. 11, 768–767. doi:10.1190/tle41110768.1.
22. Whiteley, J. S., Watlet, A., Uhlemann, S., Wilkinson, P., Boyd, J. P., Jordan, C., Kendall, J. M., and Chambers, J. E. (2021). Rapid Characterisation of Landslide Heterogeneity Using Unsupervised Classification of Electrical Resistivity and Seismic Refraction Surveys, *Engineering Geology*, Vol. 290, No. May, 106189. doi:10.1016/j.enggeo.2021.106189.
23. Martinho, E. (2023). *Electrical Resistivity and Induced Polarization Methods for Environmental Investigations: An Overview*, *Water, Air, and Soil Pollution* (Vol. 234), Springer International Publishing. doi:10.1007/s11270-023-06214-x.
24. Kusumayudha, S. B., Lestari, P., and Paripurno, E. T. (2018). Eruption Characteristic of the Sleeping Volcano, Sinabung, North Sumatera, Indonesia, and SMS Gateway for Disaster Early Warning System, *Indonesian Journal of Geography*, Vol. 50, No. 1, 70–77. doi:10.22146/ijg.17574.
25. Meju, M. A., and Le, L. (2002). Geoelectromagneticexploration For Natural Resources:Models, Case Studies and Challenges, *Surveys in Geophysics*, Vol. 23, 133–205.
26. Lange, D., Tilmann, F., Henstock, T., Rietbrock, A., Natawidjaja, D., and Kopp, H. (2018). Structure of the Central Sumatran Subduction Zone Revealed by Local Earthquake Travel-Time Tomography Using an Amphibious Network, *Solid Earth*, Vol. 9, No. 4, 1035–1049. doi:10.5194/se-9-1035-2018.
27. Lin, J. Y., Sibuet, J. C., Hsu, S. K., and Wu, W. N. (2014). Could a Sumatra-like Megathrust Earthquake Occur in the South Ryukyu Subduction Zone?, *Earth, Planets and Space*, Vol. 66, No. 1, 1–8. doi:10.1186/1880-5981-66-49.
28. Siringoringo, L. P., Sapiie, B., Rudyawan, A., and Sucipta, I. G. B. E. (2024). Origin of High Heat Flow in the Back-Arc Basins of Sumatra: An Opportunity for Geothermal Energy Development, *Energy Geoscience*, Vol. 5, No. 3, 100289. doi:10.1016/j.engeos.2024.100289.
29. Hochstein, M. P., and Sudarman, S. (1993). Geothermal Resources of Sumatra, *Geothermics*, Vol. 22, No. 3, 181–200. doi:10.1016/0375-6505(93)90042-L.